Sequential particle filter estimation of a time-dependent heat transfer coefficient in a multidimensional nonlinear inverse heat conduction problem

W. B. da Silva[1], J. C. S. Dutra[1], C. E. P. Kopperschimidt[1], D. Lesnic[2]* and R. G. Aykroyd[3]

[1] *Department of Rural Engineering, Federal University of Espírito Santo, Alegre, 29500-000, Brazil*
[2]*Department of Applied Mathematics, University of Leeds, Leeds LS2 9JT, UK*
[3]*Department of Statistics, University of Leeds, Leeds, LS2 9JT, UK*

Abstract

In the applied mathematical modelling of heat transfer systems, the heat transfer coefficient (HTC) is one of the most important parameters. This paper proposes a combination of the Method of Fundamental Solutions (MFS) with particle filter Sequential Importance Resampling (PF-SIR) to estimate the time-dependent HTC in two-dimensional transient inverse heat conduction problems from non-standard boundary integral measurements. These measurements ensure the unique solvability of the boundary coefficient identification problem. Numerical results show high performance on several test cases with both linear and nonlinear Robin boundary conditions, supporting the synergy between the MFS and simulation-based particle filter sequential analysis methods.

Keywords: Particle filter; method of fundamental solutions; inverse heat conduction; heat transfer coefficient.

1   Introduction

Several applications in science and engineering produce insufficient data to be fully described as direct problems, but can be treated as inverse problems [1]. When the main problem is related to the estimation of unknown quantities appearing in the mathematical formulation of physical processes in thermal sciences, it is called an inverse heat transfer problem. Within this framework, the estimation of the heat transfer coefficient (HTC) is a common task [2, 3, 4, 5, 6]. In thermo-metallurgical applications [7, 8], the HTC represents the most important process parameter associated with quench severity since it is closely related to the micro-structure and residual stress levels after quenching [9].

1

In the iterative solution of an inverse problem, the direct problem must be called repeatedly many times. This makes methods that do not require tedious domain discretisation, called meshless methods, more attractive. In this regard and in comparison to the more established boundary element method (BEM), the Method of Fundamental Solutions (MFS) [10] does not need any boundary discretisation and integration.

The MFS is a collocation method in which no complicated mesh needs to be generated, and this makes it relatively easy to program and computationally inexpensive. The MFS has predominantly been applied to stationary heat conduction problems governed by the Laplace or modified Helmholtz PDEs [11, 12], and it has produced accurate and stable results. The MFS for the time-dependent linear parabolic heat equation was proposed in [13], in which time-dependent fundamental solutions for parabolic PDEs were used. This approach can also be found in [14, 15, 16].

For the determination of the HTC in a two-dimensional transient heat conduction problem, Masson *et al.* [17] and Yang *et al.* [18] used the iterative conjugate gradient regularization method. The same method was used by Lu *et al.* [19] for predicting the HTC at the inner wall of a pipeline transporting a mixture of cold and hot fluids in a nuclear power plant. However, especially for nonlinear coefficient identification problems, such gradient methods requiring minimization of the distance between the estimated and the measured data can get stuck in a local minimum and, therefore, they require a good initial guess close to the true solution.

Alternatively, Yan *et al.* [20] used the Markov chain Monte Carlo (MCMC) algorithm [21] for the solution of the inverse transient heat conduction problem concerning the determination of the HTC. MCMC was shown to be a reliable method for offline problems, but it also resulted in some negative values for the HTC which are physically unrealistic. The same happened with the results of [22, 23, 24] obtained using the BEM with no positivity constraint or regularization imposed. In addition, in higher dimensions, MCMC incurs a high computational cost.

An alternative is the Bayesian filter, which has relatively low computational demands compared to the MCMC algorithm. The most widely known Bayesian filter is the Kalman filter (KF) [25], which is, however, limited to linear models with additive Gaussian noise. Extensions of the KF were developed in the past for less restrictive cases by using linearization techniques [26]. Similarly, sequential Monte Carlo methods have been developed in order to represent the posterior density in terms of random samples and associated weights. Such methods, usually denoted as particle filters, do not require the restrictive hypotheses of KF. Furthermore, particle filters can be applied to non-linear systems contaminated with any kind of noise errors [26, 27, 28, 29].

A recursive technique that uses recursive Bayesian filters, along with Monte Carlo simulations, was presented by Hammersley and Hanscomb [30]. In this approach, called the Sequential Importance Sampling (SIS), the posterior probability function is represented as a set of random samples associated with some weights. Gordon *et al.* [31] added an extra step, named re-sampling, into the SIS method to avoid a problem known as degeneration of particles leading to the Sequential Importance Re-sampling (SIR) algorithm. For the application of the particle filters to inverse heat conduction problems we refer the reader to [32, 33].

The sequential particle filter reconstruction of the HTC at the ends of a one-dimensional finite slab has recently been investigated by the authors in [34], and in this paper we consider the more realistic, but at the same time more involved and computationally complicated two-dimensional case of a heat conducting plate. Therefore, we study the sequential estimation of the time-dependent HTC in a multi-dimensional nonlinear inverse heat conduction problem, as formulated in section 2. The MFS is used to solve the direct problem sequentially for the SIR filter, as described in sec-

tions 3 and 4. Numerical results presented and discussed in section 5 indicate that this combination shows good performance in terms of robustness, stability and accuracy. Finally, section 6 presents the conclusions of our investigation.

2 Mathematical formulation

In this section, we formulate the mathematical model for the inverse problem of determining a time-dependent Robin HTC. We formulate the problem in two-dimensions, with essentially the same statements holding also in three-dimensions, but with an increase in numerical complexity of computational implementation. Given a final time of interest $t_f > 0$ and a two-dimensional bounded domain $\Omega \subset \mathbb{R}^2$ with sufficiently smooth boundary $\partial\Omega$, the aim is to find the pair $(\rho(t), T(x_1, x_2, t))$, where $T(x_1, x_2, t)$ represents the temperature for $(x_1, x_2) \in \Omega$, $t \in [0, t_f)$ and $\rho(t) \geq 0$ is the time-dependent HTC, satisfying:

$$\frac{\partial T}{\partial t}(x_1, x_2, t) = \frac{\partial^2 T}{\partial x_1^2}(x_1, x_2, t) + \frac{\partial^2 T}{\partial x_2^2}(x_1, x_2, t), \quad (x_1, x_2, t) \in \Omega \times (0, t_f), \tag{1a}$$

$$T(x_1, x_2, 0) = T^0(x_1, x_2), \quad x \in \Omega, \tag{1b}$$

$$\frac{\partial T}{\partial n}(x_1, x_2, t) + \rho(t)g(T(x_1, x_2, t)) = h(x_1, x_2, t), \quad (x_1, x_2, t) \in \partial\Omega \times [0, t_f), \tag{1c}$$

where n is the outward unit normal to the boundary $\partial\Omega$. Also, g, T^0 and h are given functions. For simplicity, the heat capacity and thermal conductivity were taken to be constant and equal to unity, whilst the heat source was assumed to be absent. In order to compensate for the missing HTC $\rho(t)$, we consider some additional information given by the non-local measurement [22, 23]

$$E(t) = \int_{\partial\Omega} \Phi(T(x_1, x_2, t))ds(x_1, x_2), \quad t \in \times[0, t_f), \tag{2}$$

where $\Phi(T) = \int g(T)dT$ is a primitive of the function g governing the linear ($g(\sigma) = \sigma$) or non-linear (e.g. radiative $g(\sigma) = \sigma^3|\sigma|$) boundary heat transfer law. The objective is to evaluate the performance of the MFS+SIR filter for estimating the time dependent HTC $\rho(t)$ at each time t for the inverse HTC identification problem (1a)-(1c) and (2). We seek the temperature $T(x_1, x_2, t)$ in the admissible set $\mathscr{T} := \left\{ T \in L_2((0, t_f); H^1(\Omega)); \partial_t T \in L_2((0, t_f); L_2(\Omega)) \right\}$ and the HTC $\rho(t)$ in the admissible set

$$\Sigma = \begin{cases} L^2((0, t_f)) \ni \rho(t) \geq 0 & \text{a.e. in } [0, T], & \text{if } g(T) \text{ is linear,} \\ 0 \leq \rho \in C^1([0, t_f]); \quad \frac{|\rho'(t)|}{\rho(t)} \leq C_0, & \forall t \in [0, t_f], & \text{if } g(T) \text{ is nonlinear,} \end{cases} \tag{3}$$

for some given constant $C_0 \geq 0$. We assume that the given input data satisfy:

(i) $T^0 \in H^2(\Omega)$, h and $\partial_t h \in L_2((0, t_f); L_2(\partial\Omega))$;

(ii) $g \in C^1(\mathbb{R}^2)$, $g(0) = 0$, $g' \geq 0$, $|g(s)| \leq C_1(|s|^\alpha + 1)$, $\forall s \in \mathbb{R}$,

for some given constants $C_1 \geq 0$ and $\alpha \geq 0$. Condition (ii) includes the case of linear convection $g(s) = s$ and the nonlinear radiation $g(s) = s^3 |s|$ for $\alpha = 1$ and $\alpha = 4$, respectively.

We have the following definition of a weak solution to the direct problem (1a)-(1c).

Definition 1. Let the input data T^0, h and g satisfy conditions (i) and (ii). Then, for any $\rho \in \Sigma$, a function $T_\rho \in \mathcal{T}$ is called a *weak solution* to the direct problem (1a)-(1c) if T_ρ satisfies the initial condition (1b) and

$$\langle \partial_t T_\rho, \varphi \rangle_\Omega + \langle \nabla T_\rho, \nabla \varphi \rangle_\Omega + \rho \langle g(T_\rho), \varphi \rangle_{\partial\Omega} = \langle h, \varphi \rangle_{\partial\Omega}, \quad \forall \varphi \in H^1(\Omega), \quad \text{a.e. in } (0, t_f), \quad (4)$$

where $\langle , \rangle$ denotes the inner product in the corresponding L_2-spaces. Using classical mathematical techniques from [35], if can be shown that the direct problem (1a)-(1c) has a unique weak solution in the context of Definition 1.

The uniqueness of the solution to the inverse problem (1a)-(1c) and (2) is given by the following theorem, [22, 23, 36].

Theorem 1. *Let the input data T^0, h and g satisfy conditions (i) and (ii). Let ρ and $\tilde{\rho}$ be in Σ and let T_ρ and $T_{\tilde{\rho}}$ be the corresponding weak solutions in $\mathcal{T}$ of (1a)-(1c) according to Definition 1. Assume further that T_ρ and $T_{\tilde{\rho}}$ also belong to $C([0, t_f]; L_2(\Omega))$. Then, if the data (2) coincide, i.e.*

$$0 < E(t) = \int_{\partial\Omega} \Phi(T_\rho(x,t)) ds(x) = \int_{\partial\Omega} \Phi(T_{\tilde{\rho}}(x,t)) ds(x), \quad \forall t \in [0, t_f],$$

then $T_\rho = T_{\tilde{\rho}}$ and $\rho = \tilde{\rho}$.

The existence of solutions to the inverse problem (1a)-(1c) and (2) is also of interest. Since the time-dependent HTC $\rho = \rho(t)$ is sought as being independent of the curvilinear coordinate along the boundary $\partial\Omega$, the following compatibility condition between (1a)-(1c) is needed:

(iii) assume that there exist a constant $\rho_* \geq 0$ and $\partial_t T_{\rho_*}(\cdot, 0) \in C(\overline{\Omega})$, such that

$$\langle \partial_t T_{\rho*}(\cdot, 0), \varphi \rangle_\Omega + \langle \nabla T_{\rho*}(\cdot, 0), \nabla \varphi \rangle_\Omega + \rho_* \langle g(T_{\rho*}(\cdot, 0)), \varphi \rangle_{\partial\Omega} = \langle h(\cdot, 0), \varphi \rangle_{\partial\Omega}, \forall \varphi \in H^1(\Omega).$$

Then, we have the following theorem establishing the existence of a solution to the inverse problem (1a)-(1c) and (2), [22, 23, 36].

Theorem 2. *Let the input data T^0, h and g satisfy conditions (i) and (ii). Assume also that condition (iii) holds and that $E \in C^2([0, t_f])$, $E'(t) \geq C_2 > 0$, $|E'(t)| \leq C_3$ for all $t \in [0, t_f]$, for some given constants C_2 and C_3, and*

$$0 < E(t) \leq \int_{\partial\Omega} \Phi(T_0(x,t)) ds(x), \quad \forall t \in [0, t_f], \quad (5)$$

where $T_0 \in \mathcal{T}$ is the unique weak solution of the direct problem (1a)-(1c) for $\rho = 0$. Then, there exists a solution $(\rho(t), T(x_1, x_2, t)) \in \Sigma \times \mathcal{T}$, which in addition satisfies this condition that $T \in C([0, t_f]; L_2(\Omega))$.

4

3 The method of fundamental solutions (MFS)

The fundamental solution to the two-dimensional heat equation (1a) is given by

$$F(\mathbf{x},t;\mathbf{y},\tau) = \frac{H(t-\tau)}{4\pi(t-\tau)}e^{-(\mathbf{x}-\mathbf{y})^2/(4(t-\tau))}, \tag{6}$$

where H is the Heaviside function, which is introduced to emphasize that the fundamental solution is zero for $t < \tau$, and when $t = \tau$. Then, based on the MFS, an approximation to the solution of Equations (1a)-(1c) can be sought as, [37, 38],

$$T_{M,N}(\mathbf{x},t) = \sum_{m=1}^{2M} \sum_{j=1}^{N} c_m^{(j)} F(\mathbf{x},t;\mathbf{y}_j,\tau_m), \quad (\mathbf{x},t) \in \Omega \times [0,t_f]. \tag{7}$$

We consider, for simplicity, that Ω is a two-dimensional disk of radius $r_0 > 0$, centred at the origin, and let us place the source points $(\mathbf{y}_j)_{j=\overline{1,N}}$ on a circle of radius $r_0 + h$ with $h > 0$, also centred at the origin. The parameter $h > 0$ can be chosen such that the error on the lateral and base surfaces is minimized [37].

We take the time points $(\tau_m)_{m=\overline{1,2M}}$ (each in the interval $(-t_f, t_f)$), as given by

$$\tau_m = \frac{2(m-M)-1}{2M}t_f, \quad m = 1,...,2M, \tag{8}$$

and using polar coordinates, we place the source points in space at

$$\mathbf{y}_j = (r_0 + h, \theta_j), \quad \theta_j = \frac{2\pi j}{N}, \quad j = 1,...,N. \tag{9}$$

In polar coordinates, (7) is now represented by

$$T_{M,N}(r,\theta,t) = \sum_{m=1}^{2M} \sum_{j=1}^{N} c_m^{(j)} F(r,\theta,t;r_0 + h,\theta_j,\tau_m). \tag{10}$$

For collocating the boundary condition (1c) we choose $t_k = \frac{k}{M}t_f$, for $k = 0,...,M$, whilst for collocating the initial condition (1b) we choose $r_l = r_0\sqrt{l/M}$ for $l = 1,...,M-1$, where the square root has been introduced to spread the points out within the domain, and not to cluster them at the centre.

We now impose the boundary and initial conditions (1b) and (1c) so that we can determine the unknown coefficients $c_m^{(j)}$ in (10). We obtain the following equations:

$$T_{M,N}(r_l,\theta_i,0) = \sum_{m=1}^{2M} \sum_{j=1}^{N} c_m^{(j)} F(r_l,\theta_i,0;r_0 + h,\theta_j,\tau_m) = T^0(r_l,\theta_i,0), \quad l = 1,...,M-1, \quad i = 1,...,N,$$

$$\tag{11}$$

$$\sum_{m=1}^{2M} \sum_{j=1}^{N} c_m^{(j)} \frac{\partial F}{\partial r}(r_0,\theta_i,t_k;r_0 + h,\theta_j,\tau_m) + \rho_k g\left(\sum_{m=1}^{2M} \sum_{j=1}^{N} c_m^{(i)} F(r_0,\theta_i,t_k;r_0 + h,\theta_j,\tau_m) \right) = h(r_0,\theta_i,t_k),$$

$$i = 1,...,N, \quad k = 0,...,M,$$

$$\tag{12}$$

where $\rho_k = \rho(t_k)$ for $k = 0, ..., M$. The above system can be written in a generic form as:

$$A(\underline{c}) = \underline{b}, \tag{13}$$

where $\underline{c} = ((c_m^{(1)})_{m=1,...,2M}, ..., (c_m^{(N)})_{m=1,...,2M})$ is the vector of $2MN$ unknowns and $\underline{b}$ is a known right-hand side vector containing the $(M-1)N$ initial values $(T^0(r_l, \theta_i, 0))_{l=1,...,M-1, \, i=1,...,N}$, and the $N(M+1)$ boundary values $(h(r_0, \theta_i, t_k))_{i=1,...,N, \, k=0,...,M}$.

A well-known issue with the MFS, [13], is that the resulting system of Eq. (13) is ill-conditioned and a straightforward inversion will produce unstable results. In order to stabilize the solution, it is usual to apply the Tikhonov regularization method and solve:

$$\min_{\underline{c}} \left\{ \|A(\underline{c}) - \underline{b}\|^2 + \lambda \|\underline{c}\|^2 \right\}, \tag{14}$$

where $\lambda \geq 0$ is a regularization parameter to be prescribed.

Note that when the boundary function is linear, e.g. $g(T) = T$, as in the Newton's law of cooling, the resulting system of Eq. (13) is linear, i.e.

$$A\underline{c} = \underline{b}, \tag{15}$$

where A is a matrix. In this case, the minimization problem (14) can be solved exactly to yield the regularized solution:

$$\underline{c}_\lambda = (A^{\mathrm{T}}A + \lambda I)^{-1}A^{\mathrm{T}}\underline{b}, \tag{16}$$

where $^{\mathrm{T}}$ denotes the transpose of a matrix and I is the identity matrix of order $2MN$.

In the inverse problem, the vector $\underline{\rho} = (\rho(t_k))_{k=1,...,M}$ is also unknown and the system of Eqs. (11) and (12) is supplemented with the additional information (2) given by

$$E(t_k) = \int_0^{2\pi} \Phi(T(1, \theta, t_k)) \, d\theta \approx \frac{2\pi}{N} \sum_{j=1}^{N} \Phi\left(T(1, \tilde{\theta}_j, t_k)\right), \quad k = 1, ..., M, \tag{17}$$

where $\tilde{\theta}_j = \frac{\pi(2j-1)}{N}$ for $j = 1, ..., N$. Note that at the initial time $t = t_0 = 0$ the compatibility condition between (1b) and (2) requires $E(0) = \int_0^{2\pi} \Phi(T_0(1, \theta)) d\theta$, so there is no need to impose (17) for $k = 0$. Instead of Eqs. (13) and (14) we have the extended versions

$$\tilde{A}(\underline{c}, \underline{\rho}) = \tilde{\underline{b}}, \tag{18}$$

and

$$\min_{(\underline{c}, \underline{\rho})} \left\{ \|A(\underline{c}, \underline{\rho}) - \tilde{\underline{b}}\|^2 + \lambda \left(\|\underline{c}\|^2 + \|\underline{\rho}\|^2 \right) \right\}, \tag{19}$$

where the vector $\tilde{\underline{b}}$ contains the vector $\underline{b}$ along with $(E(t_k))_{k=1,...,M}$, and $\tilde{A}$ is the extended operator governing Eqs. (11), (12) and (17).

4 The particle filter for the inverse problem

The solution of the inverse problem within the Bayesian framework is tackled in the form of statistical inference using the *posterior density*, based on Bayes' theorem. Let us consider the

measurement (2) (or its discretized version (17)). Then, since the data $\underline{E} = (E_k := E(t_k))_{k=1,...,M}$ contains information about the vector of unknowns $\underline{\rho} = (\rho_k)_{k=1,...,M}$, it can be used to update $\underline{\rho}$ by determining the conditional probability distribution of the unknown states $\underline{\rho}$ given the measurements $\underline{E}$.

For each $k = 1,...,M$, Bayes' theorem is stated as:

$$\pi(\rho_k | E_1, ..., E_k) = \frac{\pi(E_1, ..., E_k | \rho_k) \pi_{prior}(\rho_k)}{\pi(E_1, ..., E_k)}, \tag{20}$$

where $\pi(\rho_k | E_1, ..., E_k)$ is the *posterior density*, which is the conditional probability distribution of the unknown parameters given the measurements, $\pi_{prior}(\rho_k)$ is the *prior density*, which is the model for the unknowns that reflects all the uncertainty of the parameters without the information conveyed by the measurements, $\pi(E_1, ..., E_k | \rho_k)$ is the *likelihood function*, which is the measurement model incorporating the related uncertainties, that is, the conditional probability of the measurements given the unknown parameters, and $\pi(E_1, ..., E_k)$ is the *marginal probability density* of the measurements, which plays the role of a normalizing constant. If the measurement errors present in (2) are additive and independent Gaussian random variables, with zero mean and known covariance matrix W, the *likelihood function* can be expressed as in [26].

4.1   State estimation problem

Non-stationary, or state estimation, inverse problems [26] may be defined in the form of evolution and observation models, comprising stochastic processes. In the nonlinear problem framework, the parameter estimation procedure is often based on an approximation of the optimal filter [39]. The extended Kalman filter and its various alternatives can give good results in practice, but it suffers from lack of theoretical rigour. The particle filter offers a good alternative; in many practical cases giving better results, and its theoretical properties are becoming increasingly well-understood [39, 40]. It is particularly appealing to use particle filtering to estimate parameters in partially observed systems. For a review, see [41] where a non-Bayesian approach that consists of minimizing a given cost function, like the conditional least-squares criterion, or by maximizing the likelihood function, was employed. This approach is usually performed in batch processes, but it can also be extended to recursive procedures. In [42], the authors proposed a Bayesian approach where an augmented state variable, together with the unknown parameters, are processed by a filtering procedure. However, this method supposes that a prior law is given for the unknown parameters.

Another possibility is to use particle filter algorithms that rely on deterministic values of the model parameters. If these parameters are to be estimated simultaneously with the state variables, one option is to apply the SIR filter by mimicking the parameters as state variables with an evolution model, for example, in the form of a random walk process. The parameters are then estimated sequentially along with the state variables. Such an approach can result in accurate estimates of the parameters, even for physically complicated nonlinear problems such as in fire propagation [43].

This work applies the SIR filter to the estimation of the temperature evolution at the space points $((r_l, \theta_j)_{l=1,...,M-1; j=1,...,N})$ in addition to the boundary Robin coefficient. Thus, the augmented state vector of dimension N is given by $\mathbf{x}_k = (T(r_l, \theta_j, t_k), \rho(t_k))_{l=1,...,M-1; j=1,...,N}$ for each $k = 1,...,M$. These variables are related by means of the mathematical model given in section 2, which has to be solved for each sample particle sequentially.

The estimation problem, through the particle filter, follows the procedure stated in [44]. For each $k = 1, ..., M$, it proceeds as follows: using the measured data $\mathbf{E}_k = (E_i)_{i=1,...,k}$, N_{part} particles for the states $\left\{ \mathbf{x}_k^{(i)} \right\}_{i=1}^{N_{part}}$ are drawn from a prior probability density function (PDF). Such particles are propagated using the state evolution model and updated with the observation model in order to give the measurement estimates $\left\{ z_k^{(i)} \right\}_{i=1}^{N_{part}}$ of data (2). Afterwards, a likelihood function assigns an importance weight, $w_k^{(i)} \sim \pi(z_k^{(i)}|\mathbf{E}_k)$ for $i = 1, ..., N_{part}$. The set of the updated states and the weights $\left\{ \mathbf{x}_k^{(i)}, w_k^{(i)} \right\}_{i=1}^{N_{part}}$ represents the approximation of the posterior density.

In the current inverse problem, the evolution model for the temperature is the numerical approximation of the solution of the direct problem (1a)-(1c) through the MFS and the evolution model for the boundary Robin coefficient is a random walk. Since the measurement estimates are observations of the respective estimated states, we have the following evolution and observation models:

$$\rho_k = \rho_{k-1} + \sigma_\rho e_k, \quad k = 1, ..., M, \tag{21}$$

$$T(r_l, \theta_j, t_k) = MFS(T(r_l, \theta_j, t_{k-1}), \rho_k) + v_k, \quad k = 1, ..., M, \quad l = 1, ..., M-1, \quad j = 1, ..., N, \tag{22}$$

$$z_k = n_k + E(t_k), \quad k = 1, ..., M, \tag{23}$$

where e_k is a random variable drawn from a normal distribution with zero mean and unitary standard deviation, v_k and n_k are process and measurement noise, respectively, and $\sigma_\rho = \sigma_\rho(k)$ is a positive constant to be prescribed at each time step t_k for $k = 1, ..., M$. The subscript k on ρ denotes that the parameter will be sequentially estimated along with the state variables. To initiate the above procedure we prescribe $\mathbf{x}_0 = (T(r_l, \theta_j, 0), \rho(0))_{l=1,..,M-1; j=1,...,N}$. This is obtained by noting that at $t = t_0 = 0$, we already know $(T(r_l, \theta_j, 0) = T^0(r_l, \theta_j))$ for $l = 1, .., M-1$ and $j = 1, ..., N$ from the initial condition (1b). From the compatibility condition between (1b) and (1c) at $t = 0$ we can also infer that $\rho_0 = \rho(0) = (h(1, 0, 0) - \partial_r T^0(1, 0))/g(T^0(1, 0))$.

4.2 Particle filter algorithm

The particle filter method is a Monte Carlo technique for the solution of state estimation problems, in which the posterior density is represented by a set of particles with associated weights. After assigning the importance weights, they are normalized, so that $\sum_{i=1}^{N_{part}} w_k^i = 1$. In this regard, the Sequential Importance Sampling (SIS) algorithm estimates the posterior distribution from a set of particles representative of the system variables [27, 45]. The prior distribution provides the necessary information for the initial step: it is the basis for the first particle draw. The likelihood function is then used to compare the initial information with the experimental measurements, and incorporates more information, via particle weights, in order to determine the posterior distribution. However, the sequential application of the particle filter may result in a degeneracy phenomenon: after a few time iterations, all but a few particles have negligible weight. The degeneracy implies that a large computational effort is devoted to update particles whose contribution to the approximation of the posterior density is practically zero [27, 45]. This problem can be overcome with

a resampling step in the particle filter algorithm. Resampling involves a mapping of the random pair $\{\mathbf{x}_k^i, w_k^i\}$ into $\{\mathbf{x}_k^{i*}, N_{part}^{-1}\}$, with uniform weights. It deals with the elimination of particles originally with low weights and the replication of particles with high weights ($\mathbf{x}_k^{i*}$). This can be performed if the number of effective particles (particles with large weights) falls below a certain threshold number. Alternatively, resampling can also be applied indiscriminatly at each instant t_k, as in the Sampling Importance Resampling (SIR) algorithm [33, 43, 44, 46, 47].

5 Numerical results and discussion

In this section, we illustrate the efficiency and accuracy of the MFS combined with the particle filter SIR algorithm. To evaluate the filter performance, the maximum width of the credible interval (MWCI) [46] was determined for each estimated variable, considering the entire period of time $[0, t_f]$. In order to assess the performance of the particle filter we introduce the root-mean-square error ($RMSE_\rho$) and the relative error $Rel(\rho)$ in the HTC, defined by

$$RMSE_\rho = \sqrt{\frac{1}{M} \sum_{k=1}^{M} (\rho_k - \hat{\rho}_k)^2}, \quad Rel(\rho) = \frac{\sqrt{\sum_{k=1}^{M} (\rho_k - \hat{\rho}_k)^2}}{\sqrt{\sum_{k=1}^{M} \rho_k^2}} \times 100\%, \tag{24}$$

where ρ_k is the true value of the HTC and $\hat{\rho}_k$ is the estimated HTC.

The following 95% credible interval (*CI*), denoted as $I_{95\%}$ and defined in the parameter space, was used as an additional diagnostic of the performance of the particle filter:

$$I_{95\%} = \hat{\rho}_k \pm 1.96 \hat{\sigma}_k, \quad k = 1, ..., M, \tag{25}$$

where $\hat{\rho}_k$ represents the estimated variable and $\hat{\sigma}_k$ represents the estimated uncertainty of the particles.

It is worth stating that a narrow maximum width CI (MWCI) generally means more accurate particle filter estimation since the particles are closer to the true value. However, the MWCI should be used with caution. A narrow width could also mean that the particles approximating the posterior density are constrained to a small range of values which do not encompass the true solution. In this sense, when particle degeneration occurs, the width of the credible interval decreases drastically since all but a few particle have negligible weight. If this issue occurs frequently, the values of MWCI will be seriously compromised and will lead to erroneous conclusions about the estimation quality. One way to circumvent this detrimental effect is to consider the effective sample size [27, 48], that is, the number of particles with non-zero weight, defined by $Neff_k = \frac{1}{\sum_{i=1}^{N_{part}} (w_k^i)^2}$, for $k = 1, ..., M$. If $Neff_k$ is a low value, it indicates severe degeneration of the particle filter. Thus, this quantity was also evaluated, along with the MWCI, to ensure the best performing particle filter is identified.

In this work, the simulated measurements were defined by (2), to which additive and uncorrelated errors were applied:

$$E_a(t_k) = E(t_k) + \varepsilon_k, \quad k = 1, ..., M, \tag{26}$$

where $(\varepsilon_k)_{k=1,...,M}$ are random variables drawn from a Gaussian distribution with mean zero and the standard deviation, in which p represents the percentage of noise, given by

$$\sigma = p \times \max_{k=1,...,M} |E(t_k)|. \tag{27}$$

The computational studies for the direct and inverse problems were performed in MATLAB on a computer with Processor Intel(R) Core(TM) i5-8265U CPU @ 1.60GHz, 1800 Mhz, 4 Core, 8 Logical Processor.

5.1 Example 1 (linear law)

We consider first a benchmark test example, given by equations (1a)-(1c) and (2), we take $t_f = 1$, $r_0 = 1$, $T^0(r, \theta) = r^2 + 1$, $h(r, \theta, t) = 2 + t(2 + 4t)$, the linear law $g(T) = T$ and the measurements (2) given by

$$E(t) = \pi(2 + 4t)^2, \quad t \in [0, t_f = 1). \tag{28}$$

It can be seen that these data satisfy the conditions of uniqueness of solution given by Theorem 1. In fact, it can be verified through direct substitution that, for the above input data, the analytical solution of the inverse problem (1a)-(1c) and (2) is given by

$$T(r, \theta, t) = r^2 + 4t + 1 \tag{29}$$

and

$$\rho(t) = t. \tag{30}$$

Similar examples have been tested in [34] in one spatial dimension.

The MFS was applied with $M = 10$, $N = 20$ and $h = 10$. First, for verification, we solve the direct problem given by equations (1a)-(1c) when the HTC is assumed to be known and given by (30). Figure 1(a) compares the analytical solution for $E(t)$ given by (28) with the corresponding MFS numerical solution obtained from (7), (16) and (17) with a small regularization parameter $\lambda = 10^{-12}$. We can see the high accuracy when the MFS is used to solve the direct problem.

Next, we investigate the inverse problem (1a)-(1c) and (2). First, we consider the choice of $\sigma_\rho(k)$ in the random walk iteration (21). The number of particles N_{part} was set arbitrarily to be in increasingly doubling numbers 50, 100, 200 and 400, which led to average computational times of 95, 185, 459 and 980 seconds, respectively, to filter sequentially the measurements (26). It is important to highlight that the time to propagate each particle through the MFS was approximately 0.27 seconds.

To avoid sample degeneracy it is sufficient to keep the effective sample size over a certain threshold such as $Neff > 0.5 \cdot N_{part}$, [27]. In this regard, we propose that σ_ρ is drawn from a uniform distribution between 0.05 and 0.2. This hypothesis was adopted assuming that we know *a priori* that the maximum value of the HTC (30) is equal to unity, such that the lower limit corresponds to 5% of it. On the other hand, if the HTC suddenly changes over time, the parameter search field should be broaden, so that 20% of the maximum allowable value is used as an upper limit.

Figure 2(c) shows the behaviour of $\sigma_\rho(k)$ over the time steps t_k for $k = 1, ..., M$. It is possible to observe that, for all particle numbers tested, σ_ρ converges to approximately 0.125.

Table 1 shows the results of the evaluation criteria (24) for $p \in \{1\%, 5\%\}$ noise, in which $Neff[\%]$ denotes the average percentage ratio between the effective sample size $Neff$ and the total number of particles N_{part}. From, this table it can be seen that accurate numerical results

are obtained with relative errors $Rel(\rho) < 5\%$. Throughout the simulations there was no sample degeneration, since $Neff[\%]$ was greater than or equal to 50% for all N_{part}. Besides that, the errors (24) decrease substantially with the increase in the number of particles. Since in the behaviour of the random walk model (21) we allow σ_ρ to vary piecewise over time, the filter is able to draw particles close to the actual HTC with suitable performance even for small numbers of particles.

The numerical results for Example 1 with $N_{part} = 400$ and $p \in \{1\%, 5\%\}$ noise in the data (26) are shown in Figures 2 and 3, respectively. The shaded region denotes the 95% credible intervals, which quantifies the uncertainty of the mean. We can see that the posterior distribution mean is in excellent agreement with the true solution (30) and the credible interval shrinks as the noise level p decreases. Furthermore, the results presented in Figures 2 and 3 show clearly that the SIR particle filter approach provides stable numerical solutions to the inverse Robin problem for the heat conduction inverse problem in higher dimensions with convective boundary conditions.

5.2 Example 2 (nonlinear law)

In the second example, given by equations (1a)-(1c), we take $t_f = 1$ and $T^0(r,\theta) = r^2$, $h(r,\theta,t) = 2 + (1+t)(1+4t)^4$, the nonlinear law, $g(T) = T^3 |T|$ corresponding to radiation, and the measurements (2) given by

$$E(t) = \frac{2\pi(1+4t)^5}{5}, \quad t \in [0, t_f = 1). \tag{31}$$

In this example, the inverse problem has the analytical solution

$$T(r,\theta,t) = r^2 + 4t \tag{32}$$

and

$$\rho(t) = t + 1. \tag{33}$$

We applied the MFS with $M = 10$, $N = 10$ and $h = 1$. The solution was obtained using the *lsqnonlin* function in MATLAB with the trust-region-reflective method in order to solve the nonlinear least-squares problem caused by the nonlinearity from boundary conditions.

Figure 1(b) shows the MFS solution in comparison to the analytical solution for $E(t)$ when solving the direct problem (1a)-(1c) for Example 2 with $\rho(t)$ given by (33). We can see that the MFS produces very accurate numerical results for the direct problem.

Next, in the inverse problem, for the determination of the HTC in Example 2, we have used 50, 100, 200 and 400 particles, which led to average computational times of 710, 852, 1507 and 3357 seconds, respectively, using the measurements (26). It is important to highlight that the time to propagate each particle through the MFS was approximately 0.83 seconds. Note that CPU time has increased due to the non-linearity $g(T)$ in the boundary condition (1c).

Table 2 and Figure 4 present the numerical results obtained by inverting the data (2) contaminated with $p \in \{1\%, 5\%\}$ noise (26). It can be seen that the evaluation error criteria (24) are consistent with the error in the data and the estimated HTC lies within a credible interval of reasonable width. Figures 4(a) and 4(b) show that the behaviour of σ_ρ over the time steps t_k for $k = 1, ..., M$. It is possible to observe that, for all particle numbers tested, σ_ρ converges to approximately 0.135. The results presented in Figure 4 show clearly that of the SIR particle filter approach provides stable numerical solutions to the inverse Robin problem for heat conduction inverse problem in higher dimensions with radiative boundary conditions.

5.3 Example 3 (physical example)

We end the numerical investigation of Section 5 by considering a physical example consisting of a circular disk $\Omega = B_{\bar{r}_0}(\mathbf{0})$ centred at the origin of radius $\bar{r}_0 = 591.43 \times 10^{-4} m$ made of copper with heat capacity $C = 3439.205 kJ/(K \cdot m^3)$ and thermal conductivity $\kappa = 401 W/(K \cdot m)$ at room temperature [49]. This yields the thermal diffusivity $\alpha = \kappa/C = 1.1660 \times 10^{-4} m^2/s$. The heat conduction experiment consists of heating the circular disk for $\bar{t}_f = 30s$ from the oscillatory initial temperature

$$T^0(\bar{x}_1, \bar{x}_2) = \overline{T}_a \left[1 + \sin\left(\frac{\bar{x}_1}{\bar{r}_0} + \frac{\bar{x}_2}{\bar{r}_0} \right) \right], \quad (\bar{x}_1, \bar{x}_2) \in B_{\bar{r}_0}(\mathbf{0}),$$

where $\overline{T}_a = 27°C = 300K$ is equal to the ambient temperature. The dimensional HTC that we have to reconstruct is given by

$$\overline{\rho}(\bar{t}) = \frac{\overline{\rho}_0 \bar{t}}{\bar{t}_f},$$

where $\overline{\rho}_0 = 10^4 W/(K \cdot m^2)$. This HTC is involved in the Robin linear boundary condition (1c) with $\overline{g}(\overline{T}) = \overline{T} - \overline{T}_a$. This data gives rise to the physical model

$$\begin{cases} \frac{\partial \overline{T}}{\partial \bar{t}} = \alpha \nabla^2 \overline{T} & \text{in } B_{\bar{r}_0}(\mathbf{0}) \times (0, \bar{t}_f), \\ \overline{T}|_{\bar{t}=0} = \overline{T}^0 & \text{in } B_{\bar{r}_0}(\mathbf{0}), \\ \kappa \frac{\partial \overline{T}}{\partial n} + \overline{\rho}(\bar{t})(\overline{T} - \overline{T}_a) = \overline{h} & \text{on } \partial B_{\bar{r}_0}(\mathbf{0}) \times (0, \bar{t}_f), \end{cases} \tag{34}$$

where the heat flux (in W/m^2) is given by

$$\overline{h}(\bar{x}_1, \bar{x}_2, t) = \left[\frac{\kappa(\bar{x}_1 + \bar{x}_2)}{\bar{r}_0^2} \cos\left(\frac{\bar{x}_1}{\bar{r}_0} + \frac{\bar{x}_2}{\bar{r}_0} \right) + \overline{\rho}_0 \frac{\bar{t}}{\bar{t}_f} \sin\left(\frac{\bar{x}_1}{\bar{r}_0} + \frac{\bar{x}_2}{\bar{r}_0} \right) \right] \overline{T}_a e^{-2\bar{t}/\bar{t}_f}.$$

We also take the measured data (in $m \cdot K^2$) in (2) as

$$\overline{E}(\bar{t}) = 1.8795 \bar{r}_0 \overline{T}_a^2 e^{-4\bar{t}/\bar{t}_f}, \quad \bar{t} \in (0, \bar{t}_f). \tag{35}$$

Before performing any numerical implementation, all physical quantities in this heat conduction model are non-dimensionalised as follows:

$$t = \bar{t}/\bar{t}_f, \quad x_1 = \bar{x}_1/\bar{r}_0, \quad x_2 = \bar{x}_2/\bar{r}_0, \quad r_0 = (\bar{x}_1^2 + \bar{x}_2^2)^{1/2}/\bar{r}_0,$$

$$T = \frac{\overline{T} - \overline{T}_a}{\overline{T}_a}, \quad \rho = \frac{\overline{\rho}\bar{r}_0}{\kappa}, \quad E = \frac{\overline{E}}{\bar{r}_0 \overline{T}_a^2}, \quad h = \frac{\overline{h}\bar{r}_0}{(\overline{T}_a \kappa)}, \quad g(T) = \frac{\overline{g}(\overline{T})}{\overline{T}_a} = T.$$

With these changes of variables, the system of equations (34) and (35) becomes in non-dimensional form as follows:

$$\frac{\partial T}{\partial t}(x_1, x_2, t) = \Lambda \nabla^2 T(x_1, x_2, t), \quad (x_1, x_2, t) \in B_1(\mathbf{0}) \times (0, 1), \tag{36}$$

12

$$T(x_1, x_2, 0) = T^0(x_1, x_2) = \sin(x_1 + x_2), \quad (x_1, x_2) \in B_1(\mathbf{0}),$$

$$\frac{\partial T}{\partial n} + \rho(t)T = h(x_1, x_2, t) = [(x_1 + x_2)\cos(x_1 + x_2) + 1.4749t\sin(x_1 + x_2)]\,e^{-2t},$$

$$(x_1, x_2, t) \in \partial B_1(\mathbf{0}) \times (0, 1),$$

$$\frac{1}{2}\int_{\partial B_1(\mathbf{0})} T^2(x_1, x_2, t)\,ds(x_1, x_2) = E(t) = 1.8795e^{-4t}, \quad t \in (0, 1),$$

where $\Lambda = \alpha \bar{t}_f / \bar{r}_0^2 \approx 1$ is the Fourier number. The inverse problem (36) has the analytical solution

$$T(x_1, x_2, t) = e^{-2t}\sin(x_1 + x_2), \quad \rho(t) = 1.4749t. \tag{37}$$

When the Fourier number Λ appears in the governing equation (36), then the fundamental solution (6) changes to:

$$F(\mathbf{x}, t; \mathbf{y}, \tau) = \frac{H(t - \tau)}{4\pi\Lambda(t - \tau)} e^{-|\mathbf{x} - \mathbf{y}|^2/(4\Lambda(t - \tau))}.$$

Next, we investigate the inverse problem (1a)-(1c) and (2). The number of particles N_{part} was set arbitrarily to be 50, 100, 200 and 400, which led to average computational times of 63, 114, 285 and 560 seconds, respectively, to filter sequentially the data (26). The time to propagate each particle through the MFS was approximately 0.13 seconds. The numerical results presented in Table 3 and Figure 5 show the same trend and conclusions about good accuracy and stability of the estimates as those obtained from Table 1, and Figures 2 and 3 for Example 1.

6 Conclusions

In this paper, we have combined the SIR particle filter algorithm and the MFS to estimate the time-dependent HTC in a multi-dimensional nonlinear inverse heat conduction problem. Overall, the approach SIR + MFS has produced accurate and stable results. When radiation is present, the computational cost increases due to the nonlinearity in the corresponding boundary condition. The influence of the number of particles, as well as the measurement noise have been analysed. As expected, as the noise decreases or as the number of particles increases, the results improve, with narrow credible intervals. Also, as the number of particles increases, the results become more concentrated around the true value of the HTC. Future work will be concerned with the validation of the inverse model for the reconstruction of time-dependent HTCs from real measured data.

References

[1] A. Karageorghis, D. Lesnic, and L. Marin. A survey of applications of the MFS to inverse problems. *Inverse Problems in Science and Engineering*, 19:309–336, 2011.

[2] M. F. Valle, M. J. Colaço, and F. S. Netto. Estimation of the heat transfer coefficient by means of the method of fundamental solutions. *Inverse Problems in Science and Engineering*, 16(6):777–795, 2008.

[3] T. Abdelhamid, A. H. Elsheikh, A. Elazab, S. W. Sharshir, E. S. Selima, and D. Jiang. Simultaneous reconstruction of the time-dependent Robin coefficient and heat flux in heat conduction problems. *Inverse Problems in Science and Engineering*, 26(9):1231–1248, 2018.

[4] F. S. V. Bazán, L. Bedin, and F. Bozzoli. New methods for numerical estimation of convective heat transfer in circular ducts. *International Journal of Thermal Sciences*, 139:387–402, 2019.

[5] A. Mocerino, M. J. Colaço, F. Bozzoli, and S. Rainieri. Filtered reciprocity functional approach to estimate internal heat transfer coefficients in 2D cylindrical domains using infrared thermography. *International Journal of Heat and Mass Transfer*, 125:1181–1195, 2018.

[6] F. C. Hamilton, M. J. Colaço, R. N. Rogério, and A. J. K. Leiroz. Heat transfer coefficient estimation of an internal combustion engine using particle filters. *Inverse Problems in Science and Engineering*, 22(3):483–506, 2014.

[7] P. Le Masson, T. Loulou, and E. Artioukhine. Estimations of a 2D convection heat transfer coefficient during a metallurgical "jominy end-quench" test: comparison between two methods and experimental validation. *Inverse Problems in Science and Engineering*, 12(6):595–617, 2004.

[8] Y. Bouissa, D. Shahriari, H. Champliaud, and M. Jahazi. Prediction of heat transfer coefficient during quenching of large size forged blocks using modeling and experimental validation. *Case Studies in Thermal Engineering*, 13:100379, 2019.

[9] C. Simsir and H. Gur. A mathematical framework for simulation of thermal processing of materials: Application to steel quenching. *Turkish Journal of Engineering and Environmental Sciences*, 32:85–100, 2008.

[10] V. D. Kupradze and M. A. Aleksidze. The method of functional equations for the approximate solution of certain boundary value problems. *USSR Comput. Math. Math. Phys.*, 4:82–126, 1964.

[11] A. Bogomolny. Fundamental solutions method for elliptic boundary value problems. *SIAM Journal on Numerical Analysis*, 22:644–669, 1985.

[12] C. J. S. Alves and C. S. Chen. A new method of fundamental solutions applied to nonhomogeneous elliptic problems. *Advances in Computational Mathematics*, 23:125–142, 2005.

[13] B. T. Johansson and D. Lesnic. A method of fundamental solutions for transient heat conduction. *Engineering Analysis with Boundary Elements*, 32:697–703, 2008.

[14] N. S. Mera. The method of fundamental solutions for the backward heat conduction problem. *Inverse Problems in Science and Engineering*, 13(1):65–78, 2005.

[15] B. T. Johansson and D. Lesnic. A method of fundamental solutions for transient heat conduction in layered materials. *Engineering Analysis with Boundary Elements*, 33:1362–1367, 2009.

[16] B. T. Johansson. Properties of a method of fundamental solutions for the parabolic heat equation. *Applied Mathematics Letters*, 65:83–89, 2016.

[17] P. L. Masson, T. Loulou, and E. Artioukhine. Estimation of a 2D convection heat transfer coefficient during a test: Comparison between two methods and experimental validation. *Inverse Problems in Science and Engineering*, 12:594–617, 2004.

[18] F. Yang, L. Yan, and T. Wei. The identification of a Robin coefficient by a conjugate gradient method. *International Journal for Numerical Methods in Engineering*, 78:800–816, 2009.

[19] T. Lu, W.W. Han, P.X. Jiang, Y.H. Zhu, J. Wu, and C.I. Liu. A two-dimensional inverse heat conduction problem for simultaneous estimation of heat convection coefficient, fluid temperature and wall temperature on the inner wall of a pipeline. *Progress in Nuclear Energy*, 81:161–168, 2015.

[20] L. Yan, F. Yang, and C. Fu. Bayesian inference approach to identify a Robin coefficient in one-dimensional parabolic problems. *Journal of Computational and Applied Mathematics*, 231:840–850, 2009.

[21] A. Doucet, S. Godsill, and C. Andrieu. On sequential Monte Carlo Sampling methods for Bayesian filtering. *Statistics and Computing*, 10:197–208, 2000.

[22] M. Slodička, D. Lesnic, and T. T. M. Onyango. Determination of a time-dependent heat transfer coefficient in a nonlinear inverse heat conduction problem. *Inverse Problems in Science and Engineering*, 18:65–81, 2010.

[23] T. T. M. Onyango, D. B. Ingham, D. Lesnic, and M. Slodička. Determination of a time-dependent heat transfer coefficient non-standard boundary measurements. *Mathematics and Computers in Simulation*, 79:1577–1584, 2009.

[24] T. T. M. Onyango, D. B. Ingham, and D. Lesnic. Reconstruction of heat transfer coefficients using the boundary element method. *Computers and Mathematics with Applications*, 56(1):114–126, 2008.

[25] R. Kalman. A new approach to linear filtering and prediction problems. *ASME Journal of Basic Engineering*, 82:35–45, 1960.

[26] J. Kaipio and E. Somersalo. *Statistical and Computational Inverse Problems*. Springer-Verlag, Berlin, 2004.

[27] S. Arulampalam, S. Maskell, N. Gordon, and T. Clapp. A tutorial on particle filters for on-line non-linear/non-Gaussian Bayesian tracking. *IEEE Transactions on Signal Processing*, 50:174–188, 2001.

[28] J. Kaipio, S. Duncan, A. Seppanen, E. Somersalo, and A. Voutilainen. *Handbook of Process Imaging for Automatic Control, State Estimation for Process Imaging*. CRC Press, Boca Raton, FL, 2005.

[29] C. Andrieu, A. Doucet, S. Sumeetpal, and V. Tadic. Particle methods for charge detection, system identification and control. *Proceedings of IEEE*, 92:423–438, 2004.

[30] J. M. Hammersley and D. C. Hanscomb. *Monte Carlo Methods*. Chapman & Hall, New York, 1964.

[31] N. Gordon, D. Salmond, and A. F. M. Smith. Novel approach to nonlinear and non-Gaussian Bayesian state estimation. *Institution of Electrical Engineers*, 140:107–113, 1993.

[32] H. R. B. Orlande, M. J. Colaço, G. S. Dulikravich, F. Vianna, W. B. Silva, H. M. Fonseca, and O. Fudim. State estimation problems in heat transfer. *International Journal for Uncertainty Quantification*, 2:239–258, 2012.

[33] W. B. Silva, J. C. S. Dutra, J. M. J. Costa, L. A. S. Abreu, D. C. Knupp, and A. J. Silva Neto. A hybrid estimation scheme based on the sequential importance resampling particle filter and the particle swarm optimization (PSO-SIR). In *Computational Intelligence, Optimization and Inverse Problems with Applications in Engineering*, pages 247–261. Springer International Publishing, 2019.

[34] W.B. Silva, J. S. Dutra, C. E. P. Kopperschimidt, D. Lesnic, and R. G. Aykroyd. Sequential estimation of the time-dependent heat transfer coefficient using the method of fundamental solutions and particle filters. *Inverse Problems in Science and Engineering*, (submitted), 2019.

[35] A. Friedman. *Partial Differential Equations of Parabolic Type*. Englewood Cliffs, New Jersey, 1964.

[36] M. Slodicka and R. Van Keer. Determination of a Robin coefficient in semilinear parabolic problems by means of boundary measurements. *Inverse Problems*, 18(1):139–152, 2002.

[37] B. T. Johansson, D. Lesnic, and T. Reeve. A method of fundamental solutions for two-dimensional heat conduction. *International Journal of Computer Mathematics*, 88(8):1697–1713, 2011.

[38] J. K. Grabski. On the sources placement in the method of fundamental solutions for time-dependent heat conduction problems. *Computers and Mathematics with Applications*, 2019, (in press).

[39] F. Campillo and V. Rossi. Convolution particle filter for parameter estimation in general state-space models. *IEEE Transactions on Aerospace and Electronic Systems*, 45:1073–1072, 2009.

[40] A. Doucet, N. Freitas, and N. Gordon. *Sequential Monte Carlo Methods in Practice*. Springer, Berlin, 2001.

[41] A. Doucet and V. B. Tadic. Parameter estimation in general state–space models using particle methods. *Annals of the Institute of Statistical Mathematics*, 55:409–422, 2003.

[42] J. Liu and M. West. Combined parameter and state estimation in simulation-based filtering. In *Sequential Monte Carlo Methods in Practice. Statistics for Engineering and Information Science*, pages 197–223. Springer, 2001.

[43] W. B. Silva, M. C. Rochoux, H. R. B. Orlande, M. J. Colaço, O. Fudym, M. El-Hafi, B. Cuenot, and S. Ricci. Application of particle filters to regional-scale wildfire spread. *High Temperatures High Pressures*, 43:415–440, 2014.

[44] L. S. F. Salardani, L. P. Albuquerque, J. M. J. Costa, W. B. Da Silva, and J. C. S. Dutra. Particle filter-based monitoring scheme for simulated bio-ethylene production process. *Inverse Problems in Science and Engineering*, 27:648–668, 2018.

[45] B. Ristic, S. Arulampalam, and N. Gordon. *Beyond the Kalman Filter*. Artech House, Boston, 2004.

[46] A. C. S. R. Dias, W. B. Da Silva, and J. C. S. Dutra. Propylene polymerization reactor control and estimation using a particle filter and neural network. *Macromolecular Reaction Engineering*, 11:1–20, 2017.

[47] R. Marques, W. B. Silva, R. Hoffmann, J. S. Dutra, and F. Coral. Sequential state inference of engineering systems through the particle move-reweighting algorithm. *Computational and Applied Mathematics*, 37:220–236, 2017.

[48] J. Liu and R. Chen. Sequential Monte Carlo methods for dynamical systems. *Journal of the American Statistical Association*, 93:1032–1044, 1998.

[49] L. Zhuo, S. Meng, and F. Yi. The use of cooled axial conduction guarded probe for the measurement of transient heat flux by calibrating the unit step response. *International Journal of Heat and Mass Transfer*, 147:118850, 2020.

Table 1. Results for $p \in \{1,5\}\%$ noise for Example 1.

N_{part}	p	$RMSE_\rho$	$Rel(\rho)\%$	MWCI	$Neff[\%]$
50	1%	0.021	3.56	0.33	54.30
100	1%	0.015	2.66	0.32	50.00
200	1%	0.012	2.03	0.32	63.86
400	1%	0.009	1.56	0.34	58.40
50	5%	0.020	4.72	0.28	51.87
100	5%	0.027	3.54	0.30	50.16
200	5%	0.010	2.53	0.31	50.37
400	5%	0.015	1.70	0.32	51.41

Table 2. Results for $p \in \{1,5\}\%$ noise for Example 2.

N_{part}	p	$RMSE_\rho$	$Rel(\rho)\%$	MWCI	$Neff[\%]$
50	1%	0.080	5.24	0.38	93.88
100	1%	0.080	5.22	0.39	92.37
200	1%	0.066	4.35	0.39	92.98
400	1%	0.066	4.32	0.41	93.91
50	5%	0.093	6.09	0.39	95.17
100	5%	0.083	5.45	0.37	94.51
200	5%	0.065	4.26	0.40	94.66
400	5%	0.059	3.58	0.40	94.55

Table 3. Results for $p \in \{1,5\}\%$ noise for Example 3.

N_{part}	p	$RMSE_\rho$	$Rel(\rho)\%$	MWCI	$Neff[\%]$
50	1%	0.052	5.97	0.58	99.61
100	1%	0.039	4.53	0.55	99.72
200	1%	0.039	4.48	0.56	99.49
400	1%	0.029	3.43	0.55	99.62
50	5%	0.111	12.72	0.56	97.38
100	5%	0.087	10.01	0.57	96.71
200	5%	0.056	6.45	0.55	96.60
400	5%	0.048	5.58	0.55	97.06
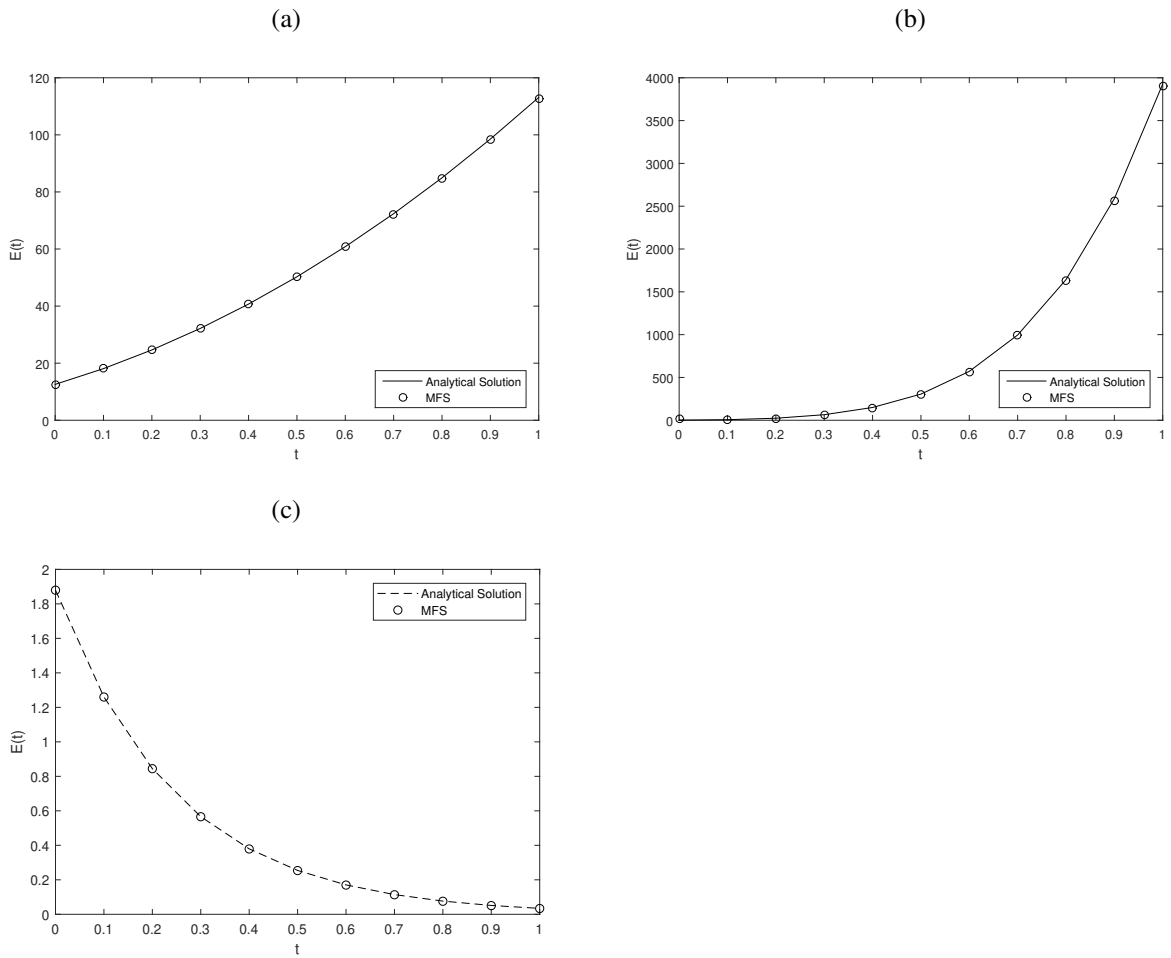
Figure 1: The analytical and MFS numerical solutions for $E(t)$, obtained when solving the direct problem for (a) Example 1, (b) Example 2 and (c) Example 3.
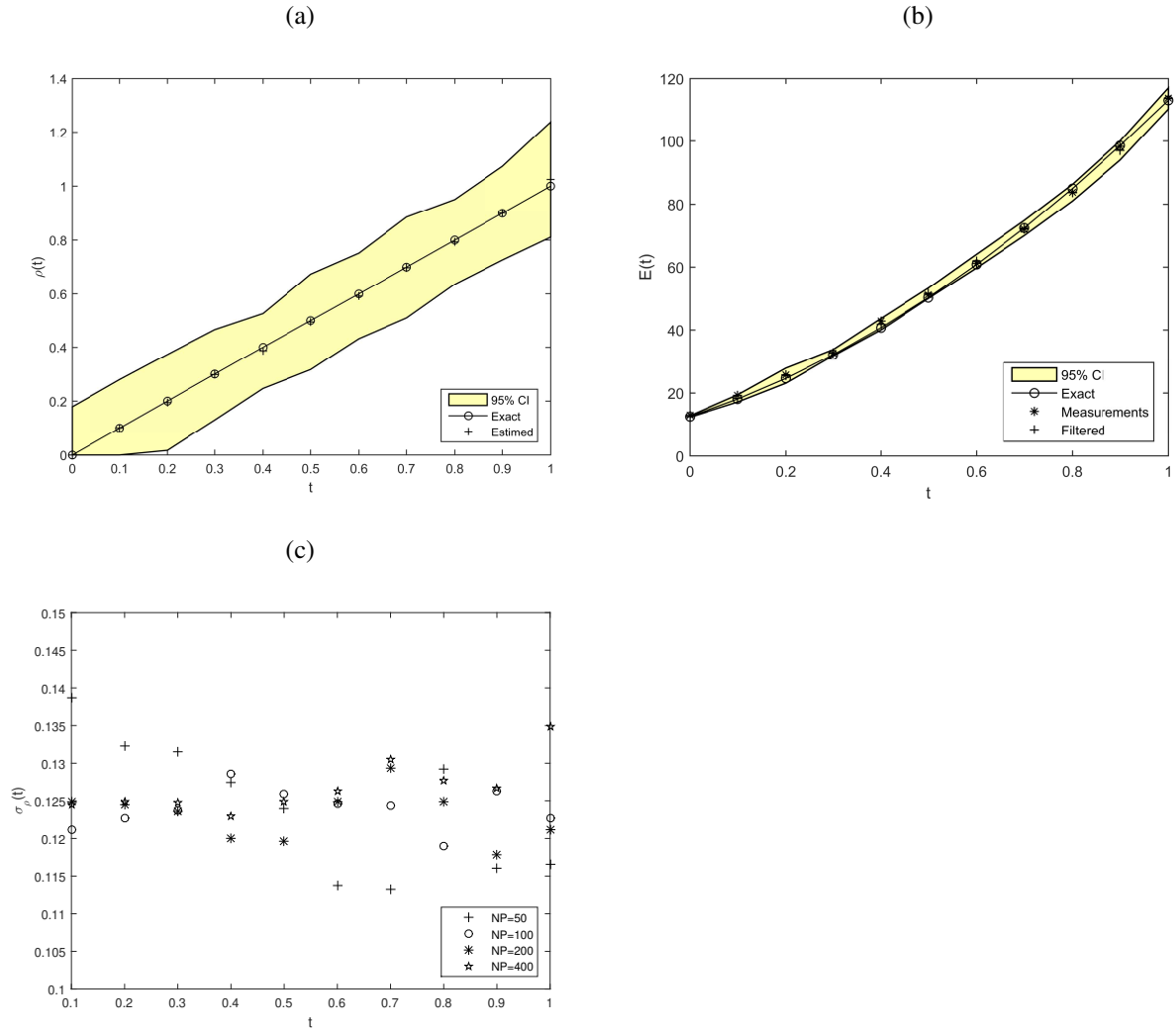
Figure 2: (a) Estimated $\rho(t)$ and (b) the filtered measurements (26) contaminated with $p = 1\%$ noise, obtained using the particle filter with $N_{part} = 400$ particles, along with (c) the behaviour of σ_ρ over time, for Example 1.

(a)

(b)

(c)
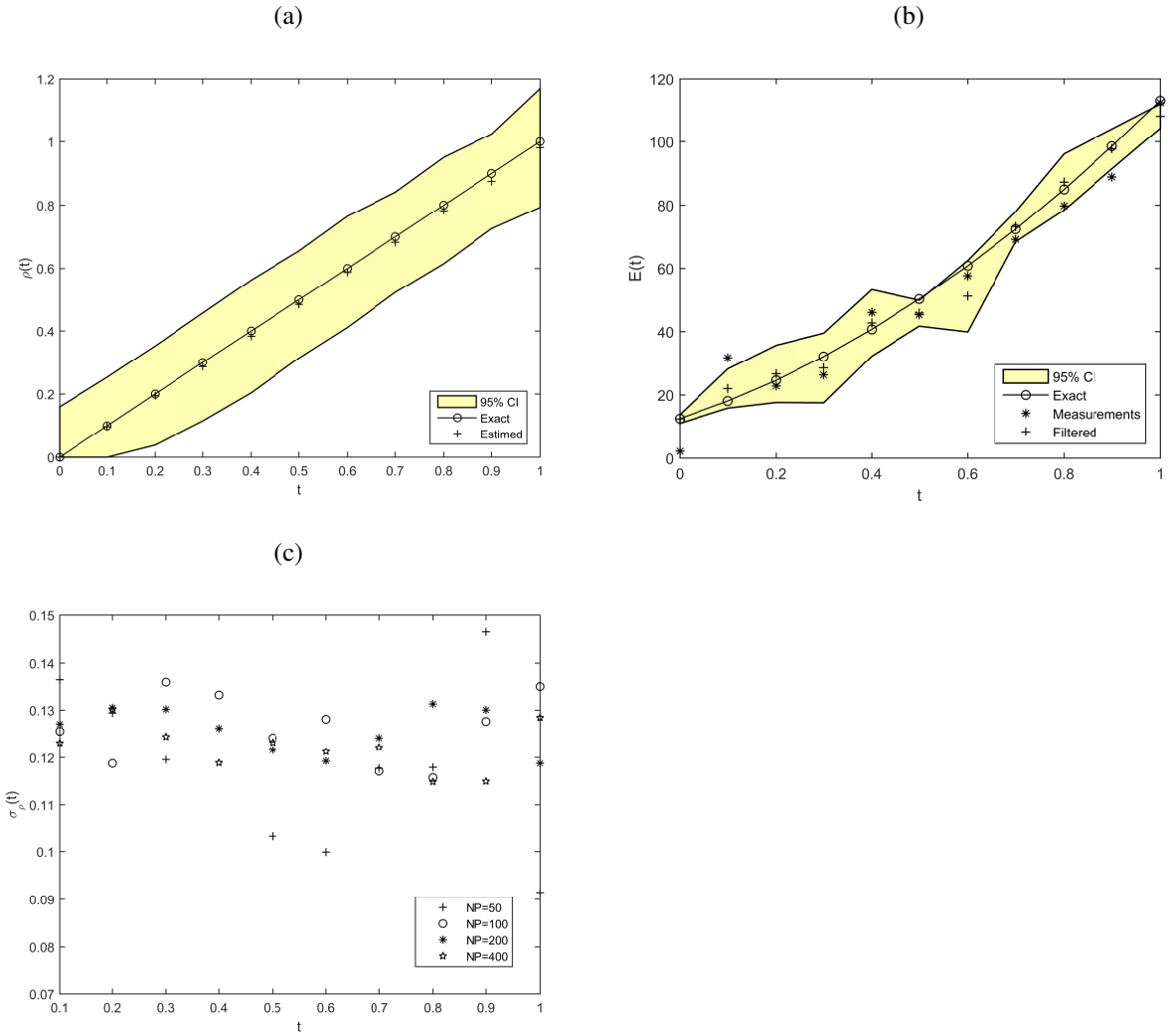
Figure 3: (a) Estimated $\rho(t)$ and (b) the filtered measurements (26) contaminated with $p = 5\%$ noise, obtained using the particle filter with $N_{part} = 400$, along with (c) the behaviour of σ_ρ over time, for Example 1.
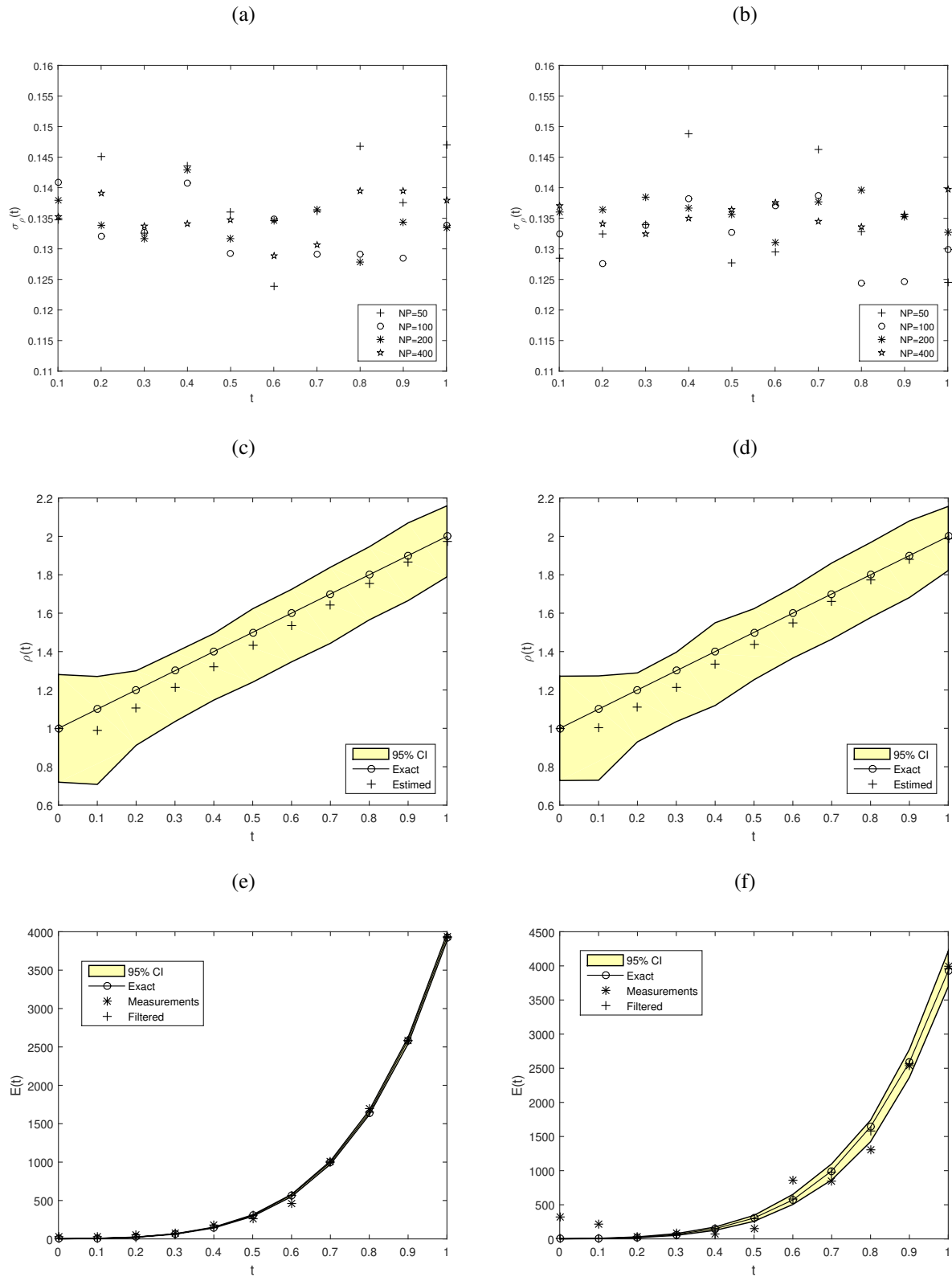
Figure 4: (a) The behaviour of σ_ρ over time for (a) $p = 1\%$ and (b) $p = 5\%$, estimated $\rho(t)$ from the measurements (26) with (c) $p = 1\%$ and (d) $p = 5\%$ noise filtered as shown in (e) and (f), respectively, obtained using the particle filter with $N_{part} = 400$ particles, for Example 2.
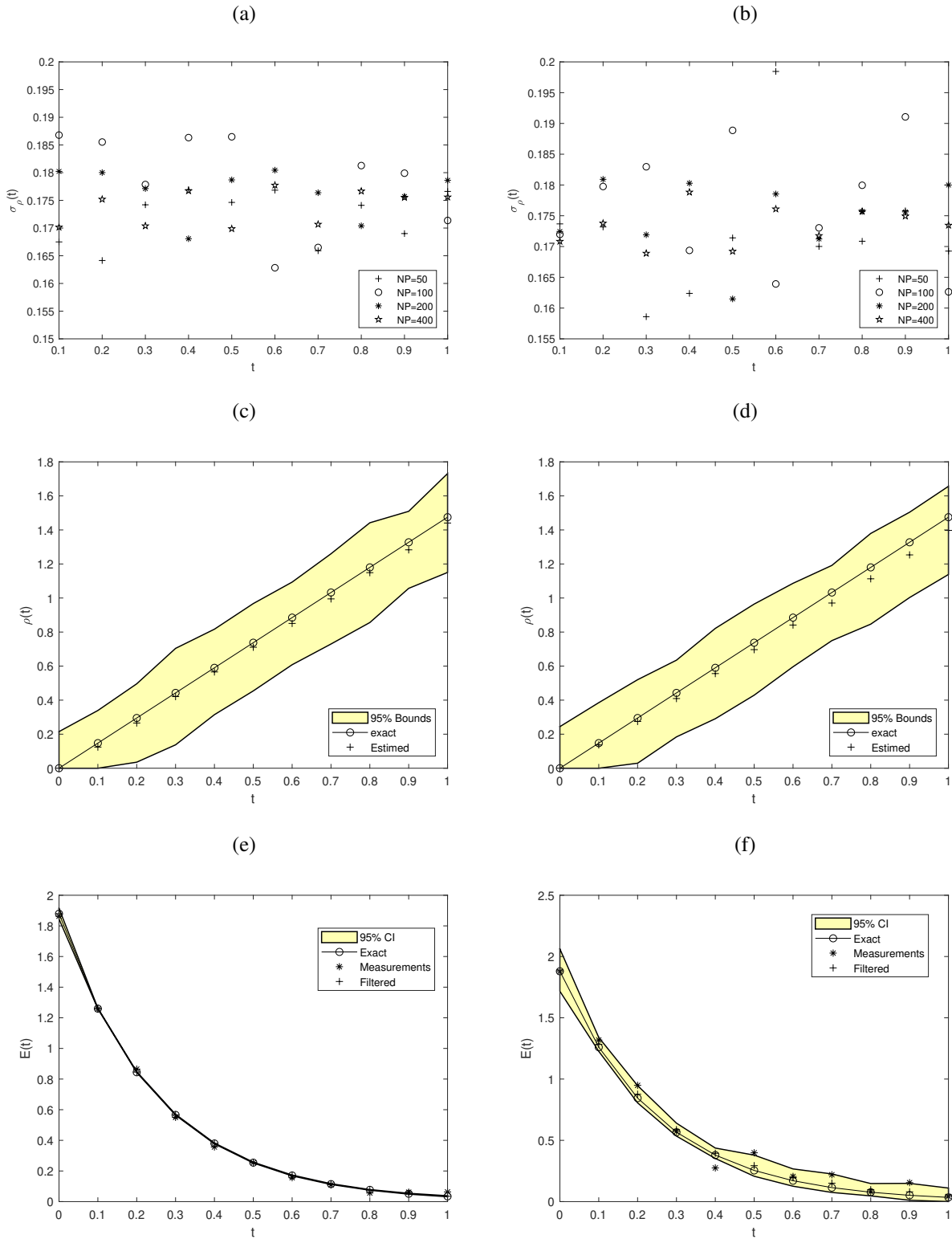
Figure 5: (a) The behaviour of σ_ρ over time for (a) $p = 1\%$ and (b) $p = 5\%$, estimated $\rho(t)$ from the measurements (26) with (c) $p = 1\%$ and (d) $p = 5\%$ noise filtered as shown in (e) and (f), respectively, obtained using the particle filter with $N_{part} = 400$ particles, for Example 3.